

# Theoretical results on a block preconditioner used in ice-sheet modeling: eigenvalue bounds for singular power-law fluids

Christian Helanow <sup>\*1</sup> and Josefin Ahlkrona <sup>†1</sup>

<sup>1</sup>Dept. Mathematics, Stockholm University, Stockholm, 106 91,  
Sweden

## Abstract

The properties of a block preconditioner that has been successfully used in finite element simulations of large scale ice-sheet flow is examined. The type of preconditioner, based on approximating the Schur complement with the mass matrix scaled by the variable viscosity, is well-known in the context of Stokes flow and has previously been analyzed for other types of non-Newtonian fluids. We adapt the theory to hold for the regularized constitutive (power-law) equation for ice and derive eigenvalue bounds of the preconditioned system for both Picard and Newton linearization using *inf-sup* stable finite elements. The eigenvalue bounds show that viscosity-scaled preconditioning clusters the eigenvalues well with only a weak dependence on the regularization parameter, while the eigenvalue bounds for the traditional non-viscosity-scaled mass-matrix preconditioner are very sensitive to the same regularization parameter. The results are verified numerically in two experiments using a manufactured solution with low regularity and a simulation of glacier flow. The numerical results further show that the computed eigenvalue bounds for the viscosity-scaled preconditioner are nearly independent of the regularization parameter. Experiments are performed using both Taylor-Hood and MINI elements, which are the common choices for *inf-sup* stable elements in ice-sheet models. Both elements conform well to the theoretical eigenvalue bounds, with MINI elements being more sensitive to the quality of the meshes used in glacier simulations.

---

<sup>\*</sup>Corresponding author: christian.helanow@math.su.se

<sup>†</sup>ahlkrona@math.su.se

# 1 Introduction

Glacial ice, as a non-Newtonian fluid, is characterized by having a variable viscosity that is dependent on the shear rate, that is the viscosity is a function of the fluid deformation. Numerical simulation of non-Newtonian fluids is challenging since the varying viscosity makes the equations governing the flow non-linear and the problem possibly ill-conditioned Leng et al. [2012]. On the discrete level the non-linearity introduced by the solution-dependent viscosity is commonly handled by linearizing the problem using the Picard or Newton method. In each Picard or Newton step a linear system has to be solved which, in the case of using iterative solvers, typically requires special preconditioning methods.

This paper focuses on modeling the non-Newtonian flow of ice, which most commonly is considered to be a gravity-driven flow of a very viscous shear-thinning power-law fluid. We study the preconditioning of the Stokes equations, which govern the steady creeping flow of ice, using a constitutive equation for which the viscosity,  $\nu$ , follows the relation

$$\nu = \nu_0(\varepsilon^2 + |\mathbf{D}\mathbf{u}|^2)^{\frac{p-2}{2}}. \quad (1)$$

Here  $\mathbf{u}$  is the velocity,  $\mathbf{D}\mathbf{u} = \frac{1}{2}(\nabla\mathbf{u} + \nabla\mathbf{u}^\top)$  is the strain-rate tensor,  $|\mathbf{D}\mathbf{u}|^2 = \mathbf{D}\mathbf{u} : \mathbf{D}\mathbf{u} = D_{ij}D_{ij}$ ,  $\nu_0$  and  $p$  are scalar material parameters, and  $\varepsilon$  is a regularization parameter.

In the case of glacial ice, standard values for the material parameters are  $p = 4/3$  and  $\varepsilon = 0$  [e.g., Glen, 1955, Cuffey and Paterson, 2010]. For such shear-thinning flow ( $p < 2$ ), we have that  $\nu \rightarrow \infty$  when  $|\mathbf{D}(\mathbf{u})| \rightarrow 0$ , making the Stokes equations a singular power-law system Hirn [2013].

It is important to improve the numerical methods for modeling the ice sheets on Greenland and Antarctica as such models are important tools in improving our understanding of the consequences of climate change [Pörtner et al., 2019, Seroussi et al., 2020]. For such large-scale simulations direct solvers, which sometimes have been used for both small and large problems [e.g., Rückamp et al., 2022, Seddik et al., 2012], become memory inefficient and iterative solvers are preferable. Recently various preconditioned iterative solvers have been used in the context of ice-sheet modeling, such as domain decomposition using an overlapping additive Schwarz method, Vanka algorithm or ILU Rückamp et al. [2022], Zhang et al. [2011]. A viscosity-scaled block preconditioner has been used in Leng et al. [e.g., 2012] and, in particular, in Schannwell et al. [2020] where the preconditioner was successfully applied to realistic ice-sheet problems using the finite element model Elmer/Ice [Gagliardini et al., 2013b].

The focus of this study is to investigate this type of block-preconditioner and to derive theoretical bounds for eigenvalues of the preconditioned algebraic system. Such block preconditioners have previously been analyzed theoretically for other types of non-Newtonian flow in Grinevich and Olshanskii [2009] (for Picard iterations) and He et al. [2015] (for Newton iterations). In these studies the viscosity was considered to be of the form

$$\nu_{min} + \nu, \quad (2)$$

where  $\nu_{min} > 0$  is a constant scalar material parameter. For the case  $p = 1$  this is the regularized Bingham model. Many of the estimates derived in [Grinevich and Olshanskii, 2009, He et al., 2015] explicitly depend on  $\nu_{min}$  and require a non-zero  $\nu_{min}$  so that the viscosity is bounded from below.

We adapt the work of Grinevich and Olshanskii [2009] and He et al. [2015] to non-Newtonian fluids with a viscosity of the form Eq. (1), i.e.  $\nu_{min} = 0$  in Eq. (2), by in part using results from Hirn [2013] specific to power-law fluids of type Eq. (1). Our results are validated in numerical experiments, both for a low-regularity manufactured solution and for a typical ice-modeling benchmark experiment. We work in a finite element setting and consider both Picard and Newton linearization.

The paper is structured as follows: Section 2 presents the problem formulation and the equations governing the flow of ice. Section 3 introduces the viscosity-scaled block preconditioner and summarizes previous related results. Section 4 presents bounds on the condition number of the preconditioned system and compares them to a classical non-viscosity-scaled preconditioner. In Section 5 the theoretical results are verified numerically with two experiments: a manufactured solution of low regularity [Belenki et al., 2012] and a problem from the ice-sheet modeling benchmark test suite ISMIP-HOM [Pattyn et al., 2008]. Finally, Section 6 presents a summary with discussion and conclusions.

## 2 Problem Formulation

### 2.1 Governing Equations

The  $p$ -Stokes equations with Dirichlet boundary conditions are

$$-\nabla\pi + \nabla \cdot \mathbf{S}(\mathbf{u}) + \mathbf{f} = \mathbf{0} \quad \text{in } \Omega, \quad (3a)$$

$$\nabla \cdot \mathbf{u} = 0 \quad \text{in } \Omega, \quad (3b)$$

$$\mathbf{u} = \mathbf{g} \quad \text{on } \Gamma, \quad (3c)$$

where  $\mathbf{u} = (u_1, \dots, u_d)$  is the  $d$ -dimensional velocity field,  $\pi$  is the pressure,  $\mathbf{f}$  is a body force and  $\mathbf{g}$  is the velocity at the boundary which must fulfill  $\int_{\Gamma} \mathbf{g} \cdot \mathbf{n} = 0$  as to not violate the divergence constraint. The domain  $\Omega \subset \mathbb{R}^d$  is open and bounded with a boundary  $\Gamma$ . In order to obtain a unique pressure we require that  $\int_{\Omega} \pi \, dx = 0$ . As opposed to the Stokes equations, the stress tensor  $\mathbf{S}(\mathbf{u})$  is non-linear due to the non-linear viscosity. The regularized constitutive equation is given as:

$$\mathbf{S}(\mathbf{u}) = \nu(\mathbf{Du})\mathbf{Du}, \quad (4)$$

$$\nu := \nu(\mathbf{Du}) = \nu_0(\varepsilon^2 + |\mathbf{Du}|^2)^{\frac{p-2}{2}}, \quad p \in (1, 2]. \quad (5)$$

The weak formulation of the  $p$ -Stokes problem is to find velocity and pressure  $(\mathbf{u}, \pi) \in \mathcal{V} \times \mathcal{Q}$  so that

$$(\mathbf{S}(\mathbf{u}), \mathbf{Dv})_{\Omega} - (\nabla \cdot \mathbf{v}, \pi)_{\Omega} - (\nabla \cdot \mathbf{u}, q)_{\Omega} = (\mathbf{f}, \mathbf{v})_{\Omega} \quad \forall (\mathbf{v}, q) \in \mathcal{V} \times \mathcal{Q}, \quad (6)$$

where we have used  $(\cdot, \cdot)_{\Omega}$  to denote the  $L^2$  scalar product, e.g.,  $(\mathbf{u}, \mathbf{v})_{\Omega} = \int_{\Omega} \mathbf{u} \cdot \mathbf{v} \, dx$ . Appropriate spaces for the continuous problem are the Sobolev space  $\mathcal{V} := [W_{\mathbf{g}}^{1,p}(\Omega)]^d$  and Lebesgue space  $\mathcal{Q} := L_0^{p'}(\Omega) := \{L^{p'}(\Omega) : (\pi, 1) = 0\}$ , where  $p' = p/(p-1)$  [see e.g., Hirn, 2013]. However, if an assumption is made that  $\mathbf{Du} \in L^{\infty}(\Omega)$ , we can seek the solution in  $\mathcal{V} := [H_{\mathbf{g}}^1(\Omega)]^d$  and  $\mathcal{Q} := L_0^2(\Omega)$ . This amounts to for the discrete problem, resulting from linearizing Eq. (6), having all iterates  $\mathbf{Du}^k \in L^{\infty}(\Omega)$  and considering each linear step as a Stokes problem with spatially variable viscosity.

**Remark 1.** When considering the flow of ice, the body force in Eq. (3a) is  $\mathbf{f} = \rho \hat{\mathbf{g}}$ , where  $\rho$  is the density of ice and  $\hat{\mathbf{g}}$  is the gravitational acceleration. The constitutive equation for ice, called Glen's flow law [Glen, 1955], is typically expressed as (cf. Eq. (4)):

$$\mathbf{S} = 2\nu_0 D_{II}^{\frac{p-2}{2}} \mathbf{Du},$$

where  $D_{II} = \frac{1}{2} \mathbf{D}_{ij} \mathbf{D}_{ij} = \frac{1}{2} \text{Tr}(\mathbf{D}^2 \mathbf{u})$  is the second invariant of the strain-rate tensor,  $\mathbf{Du}$ . Furthermore, stress-free (natural) boundary conditions and no-slip or slip conditions apply at the ice/atmosphere and ice/bedrock interface, respectively, see Fig. 1. These conditions are explained in more detail in Section 5.

## 2.2 Linearization

The problem is solved iteratively by using either the Picard or Newton method to linearize Eq. (6), resulting in a weak formulation where the viscosity depends on a known velocity from either a guess or a velocity solved

for in the previous iteration. These methods can be seen as the linearization of the continuous problem. In particular, the non-linear form

$$a(\mathbf{u})(\mathbf{v}) := (\mathbf{S}(\mathbf{u}), \mathbf{D}\mathbf{v})_\Omega = \int_\Omega \nu_0 (\varepsilon^2 + |\mathbf{D}\mathbf{u}|^2)^{\frac{p-2}{2}} \mathbf{D}\mathbf{u} : \mathbf{D}\mathbf{v} \, d\mathbf{x} \quad (7)$$

which appears in Eq. (6) is linearized as

$$\begin{aligned} a'(\mathbf{u}^k)(\delta\mathbf{u}, \mathbf{v}) &= \int_\Omega \nu_0 (\varepsilon^2 + |\mathbf{D}\mathbf{u}^k|^2)^{\frac{p-2}{2}} \mathbf{D}\delta\mathbf{u} : \mathbf{D}\mathbf{v} \, d\mathbf{x} \\ &+ \gamma(p-2) \int_\Omega \nu_0 (\varepsilon^2 + |\mathbf{D}\mathbf{u}^k|^2)^{\frac{p-4}{2}} (\mathbf{D}\mathbf{u}^k : \mathbf{D}\delta\mathbf{u})(\mathbf{D}\mathbf{u}^k : \mathbf{D}\mathbf{v}) \, d\mathbf{x}, \end{aligned} \quad (8)$$

where  $\mathbf{u}^k$  is the velocity at the  $k$ :th non-linear iteration, known from the previous iteration or an initial guess, and  $\gamma \in \{0, 1\}$ . In the linearized problem the update to the velocity  $\delta\mathbf{u} \in \mathcal{V}$  is solved for in each iteration, giving the next velocity iteration as  $\mathbf{u}^{k+1} = \mathbf{u}^k + \delta\mathbf{u}$ . For  $\gamma = 1$  Eq. (8) equals the Gâteaux derivative of  $a(\cdot)(\cdot)$  at  $\mathbf{u}^k$  in the direction of  $\delta\mathbf{u}$  [e.g., Hirn, 2013] which gives the Newton method, while  $\gamma = 0$  instead results in the Picard method (fixed point iterations).

If we let  $b(\mathbf{u}, \pi) = -(\nabla \cdot \mathbf{u}, \pi)_\Omega$  and  $(\mathbf{u}^k, \pi^k)$  be a known velocity-pressure pair, the linearized continuous problem reads: in the  $k$ :th non-linear iteration find the velocity and pressure update  $(\delta\mathbf{u}, \delta\pi) \in \mathcal{V} \times \mathcal{Q}$  so that

$$\begin{aligned} a'(\mathbf{u}^k)(\delta\mathbf{u}, \mathbf{v}) + b(\mathbf{v}, \delta\pi) + b(\delta\mathbf{u}, q) = \\ (\mathbf{f}, \mathbf{v})_\Omega - a(\mathbf{u}^k, \mathbf{v}) - b(\mathbf{v}, \pi^k) - b(\mathbf{u}^k, q) \quad \forall (\mathbf{v}, q) \in \mathcal{V} \times \mathcal{Q}. \end{aligned} \quad (9)$$

The updated solution to be used in the  $k+1$  iteration is then set to be  $(\mathbf{u}^{k+1}, \pi^{k+1}) = (\mathbf{u}^k + \delta\mathbf{u}, \pi^k + \delta\pi)$ .

In the above, if  $\mathbf{D}\mathbf{u}^k \in L^\infty(\Omega)$ , it is sufficient to use the spaces  $\mathcal{V} := [H_{\mathbf{g}}^1(\Omega)]^d$  and  $\mathcal{Q} := L_0^2(\Omega)$ , instead of the spaces specified for the continuous non-linear problem in Eq. (6). In the case of the discretized problem, this is valid as long as a (discrete) solution for  $\mathbf{u}^k$  has been found in the previous iteration.

### 2.3 Discretization

Equation (9) is discretized by triangulating the domain  $\Omega$  and seeking a discrete solution  $(\mathbf{u}_h, \pi_h) \in V_h \times Q_h$ , where  $V_h$  and  $Q_h$  are a pair of finite-dimensional spaces. We in this study employ conforming finite elements, i.e.,

$V_h \subset \mathcal{V}$  and  $Q_h \subset \mathcal{Q}$ , that satisfy the so-called *inf-sup* or LBB (Ladyzhenskaya-Babuška-Brezzi) condition [Babuška, 1973, Brezzi, 1974]:

$$c_0 \leq \inf_{p_h \in Q_h} \sup_{\mathbf{u}_h \in V_h} \frac{(\nabla \cdot \mathbf{u}_h, \pi_h)}{\|\mathbf{u}_h\|_{V_h} \|\pi_h\|_{Q_h}}, \quad (10)$$

where  $c_0$  is a positive scalar. Specifically we choose  $V_h$ ,  $Q_h$  to correspond to Taylor-Hood  $P2P1$  [Taylor and Hood, 1974] or MINI elements [Baiocchi et al., 1993], as these are *inf-sup* stable elements that are used in the numerical ice-sheet model Elmer/Ice [Schannwell et al., 2020, Gagliardini et al., 2013a].

For a unique weak solution to exist to the continuous problem Eq. (6), the *inf-sup* condition that needs to be satisfied involves the norms defined by the Sobolev spaces  $W^{1,p}$  and  $L^{p'}$  and monotonicity properties of the constitutive equation Eq. (5) [Hirn, 2013]. However, with the assumptions on the strain-rate tensor, we here follow [Grinevich and Olshanskii, 2009, He et al., 2015] and use the norms induced by the inner products on the Hilbert spaces  $H_0^1$  and  $L^2$  with the motivation provided in Section 2.2.

Let  $\{\varphi_i\}_{i=1}^n$  and  $\{\psi_i\}_{i=1}^m$  be the bases for  $V_h$  and  $Q_h$ , respectively, and let  $u_h = (u_1, \dots, u_n)^\top \in \mathbb{R}^n$  and  $\pi_h = (\pi_1, \dots, \pi_m)^\top \in \mathbb{R}^m$  represent the discrete values such that  $\delta \mathbf{u}_h = \sum_{i=1}^n u_i \varphi_i$  and  $\delta \pi_h = \sum_{i=1}^m \pi_i \psi_i$ , respectively. We can then formulate the discrete system in each iteration as

$$\begin{bmatrix} A & B^\top \\ B & 0 \end{bmatrix} \begin{bmatrix} u \\ \pi \end{bmatrix} = \begin{bmatrix} F \\ 0 \end{bmatrix}, \quad (11)$$

with

$$A_{i,j} := a'(\mathbf{u}_h^k)(\varphi_j, \varphi_i) \quad (12)$$

$$B_{i,j} := -(\nabla \cdot \varphi_i, \psi_j), \quad (13)$$

where  $F$  is the discrete representation of the right-hand side in Eq. (9) and  $a'$  depends on a known velocity  $\mathbf{u}_h^k \in V_h$  and is understood to be defined using  $\gamma = 0$  for the Picard method and  $\gamma = 1$  for the Newton method, see Eq. (8).

### 3 Preconditioning

Several types of preconditioners for non-Newtonian, variable-viscosity Stokes flow exist in the literature with, in particular, a focus on geodynamics [e.g.

May et al., 2015, Rudi et al., 2017, Fraters et al., 2019, Shih et al., 2021] and some directly related to ice-sheet models [Isaac et al., 2015].

In this study we choose, in part motivated by the successful but heuristic application in the ice-sheet model Elmer/Ice, to precondition the linear system Eq. (11) with a left block preconditioner of the form

$$P = \begin{bmatrix} \tilde{A} & 0 \\ B & -\tilde{S} \end{bmatrix} \quad (14)$$

where  $\tilde{A}$  is an approximation to  $A$  and  $\tilde{S}$  is an approximation to the Schur complement  $S = BA^{-1}B^\top$ . The approximation  $\tilde{A}$  can be found with an inexact solver, while finding an appropriate  $\tilde{S}$  is more intricate given that  $S$  is implicitly defined by  $A^{-1}$  and  $B$  and cannot be expected to be a sparse matrix. A good choice for  $\tilde{S}$  has the property that the eigenvalues of  $\tilde{S}^{-1}S$  are well clustered. For a constant viscosity (Newtonian), linear problem, the pressure mass matrix  $M$ , defined as

$$M_{i,j} := (\psi_i, \psi_j), \quad (15)$$

is a good choice for  $\tilde{S}$  as it is spectrally equivalent to the Schur complement [e.g. Elman et al., 2005].

For variable-viscosity power-law fluids, the viscosity-scaled mass matrix  $M_\nu$ , defined as

$$M_{\nu,i,j} := \left( \frac{1}{\nu} \psi_i, \psi_j \right), \quad (16)$$

is a more appropriate choice for  $\tilde{S}$ . This type of block preconditioner is used in Elmer/Ice for the shear-thinning power-law flow of ice sheets, but as part of a right preconditioner, i.e.,  $\begin{bmatrix} \tilde{A} & B^\top \\ 0 & -M_\nu \end{bmatrix}$  [Malinen et al., 2012, Råback et al., 2022]. This block preconditioner  $\tilde{S} = M$  is, together with the classical choice  $\tilde{S} = M$ , analyzed in Grinevich and Olshanskii [2009] (for the Picard method) and He et al. [2015] (for the Newton method) for a viscosity of the form Eq. (2) assuming  $\nu_{min} > 0$ .

Essential to both studies to derive a lower bound for the eigenvalues of  $M_\nu^{-1}S$  is the following auxiliary *inf-sup* condition

$$c_\nu \leq \inf_{\pi \in L_\nu} \sup_{\mathbf{u} \in H_0^1} \frac{(\nabla \cdot \mathbf{u}, \pi)}{\|\nu^{1/2} \mathbf{D}\mathbf{u}\| \|\nu^{-1/2} \pi\|}, \quad (17)$$

where  $c_\nu$  is a mesh-independent constant that only weakly depends on the regular *inf-sup* constant  $c_0$  and  $\nu$ , and indirectly on  $\varepsilon$  through the dependence of  $\nu$ . The condition is proven in Grinevich and Olshanskii [2009] for

$\pi \in L_\nu^2 := \{\pi \in L^2 : (\pi, \nu^{-1}) = 0\}$  with the additional condition that  $(\pi, \nu^{-1/2}) = 0$ . Using this *inf-sup* condition it is possible to improve the lower bound for the smallest eigenvalue of  $M_\nu^{-1}S$ : without Eq. (17) (using the LBB condition in Eq. (10)) the lower bound depends directly on the  $\varepsilon$ .

Although the conditions under which Eq. (17) is valid may not be the most general, theoretical and numerical results from Grinevich and Olshanskii [2009] indicate that  $M_\nu$  should have better preconditioning properties than implied by the directly  $\varepsilon$ -dependent lower eigenvalue bound found using Eq. (10).

The eigenvalue bounds for  $\tilde{S}^{-1}S = M^{-1}S$  depend on the material parameter  $\nu_{min}$  as

$$\frac{c_0^2}{\nu_{max}} \leq \lambda \leq \frac{1}{\nu_{min}}, \quad (18)$$

for both Picard and Newton iterations, and for  $\tilde{S}^{-1}S = M_\nu^{-1}S$  as

$$c_\nu^2 \leq \lambda \leq d \quad \text{and} \quad c_\nu^2 \leq \lambda \leq \frac{\nu_{max}}{\nu_{min}} \quad (19)$$

for Picard and Newton iterations, respectively [Grinevich and Olshanskii, 2009, He et al., 2015].

These bounds cannot be directly be used for shear-thinning power laws with a viscosity of the form Eq. (5) since there is explicit dependence on  $\nu_{min}$ . The main prospect of this paper is therefore to derive bounds for such power-law fluids. In particular, we are interested in how these bounds depend on the regularization parameter  $\varepsilon$  as it gets small, as the constitutive equation conventionally used for the creep of ice amounts to  $\varepsilon = 0$  in Eq. (5) [Glen, 1955, Duval, 1977, Duval et al., 1983].

## 4 Theoretical Results

In this section we show bounds for the eigenvalues of  $\tilde{S}^{-1}S$  for both the classical choice  $\tilde{S} = M$ , as well as for  $\tilde{S} = M_\nu$ . The bounds depend on the *inf-sup* constant  $c_0$  (see Eq. (10)) and on the constant  $c_\nu$  (see Eq. (17)). These constants are determined numerically using the methods described in Section 4.1.

Since we are considering  $\mathbf{u} \in H_0^1$  (pure Dirichlet boundary conditions) the Schur complement  $S$  has a kernel consisting of the constant vector corresponding to the constant pressure mode, which results in a zero eigenvalue. However, since this is in practice circumvented numerically by either setting an additional constraint on the pressure (e.g.,  $\int_\Omega \pi \, dx = 0$ ) or by setting a



null space for the linear system, we below treat  $S$  as non-singular and  $B$  as full rank.

To facilitate the structure of the proof of Proposition 1, we first list an assumption and some useful inequalities.

**Assumption 1.** *The following assumption is made on the deformation tensor:*

$$\mathbf{Du}^k \in L^\infty(\Omega).$$

**Lemma 1.** *The following inequalities involving the strain-rate tensor hold:*

- (i)  $\|\nabla \cdot \mathbf{u}\| \leq \|\mathbf{Du}\| \leq \|\nabla \mathbf{u}\| \quad \forall \mathbf{u} \in H_0^1(\Omega)$
- (ii)  $\|\nu^{1/2} \nabla \cdot \mathbf{u}\| \leq \sqrt{d} \|\nu^{1/2} \mathbf{Du}\| \quad \forall \mathbf{u} \in H^1(\Omega),$   
where  $d$  is the dimension.

*Proof.* (i) See e.g., Grinevich and Olshanskii [2009], John [2016]  
(ii) See Kaiser [2014].

□

**Lemma 2.** *For the viscous term of the Gâteaux derivative, Eq. (8), the following hold:*

- (i)  $a'(\mathbf{u}^k)(\mathbf{u}, \mathbf{u}) \geq (1 + \gamma(p - 2)) \|\nu_k^{1/2} \mathbf{Du}\|^2$  and  
 $a'(\mathbf{u}^k)(\mathbf{u}, \mathbf{u}) \geq (1 + \gamma(p - 2)) \nu_0 (\varepsilon^2 + \|\mathbf{Du}^k\|_\infty^2)^{\frac{p-2}{2}} \|\mathbf{Du}\|^2, \forall \mathbf{u} \in H_0^1(\Omega),$   
where  $\nu_k = \nu(\mathbf{Du}^k)$ .
- (ii)  $a'(\mathbf{u}^k)(\mathbf{u}, \mathbf{u}) \leq \int_\Omega \nu_k |\mathbf{Du}|^2 dx = \|\nu_k^{1/2} \mathbf{Du}\|^2 \leq \nu_{max} \|\mathbf{Du}\|^2,$   
where  $\nu_{max} = \nu(\mathbf{0}) = \nu_0 \varepsilon^{p-2}$ .

*Proof.* The outline of this proof can be deduced from adding intermediate steps to a proof from Hirn [2013].

(i) Noting that for  $\gamma \geq 0$  and  $p \leq 2$  the second term in Eq. (8) is always non-positive, applying Cauchy-Schwartz inequality and using that  $|\mathbf{Du}^k|^2 <$

$(\varepsilon^2 + |\mathbf{D}\mathbf{u}^k|^2)$ , we have that

$$\begin{aligned}
a'(\mathbf{u}^k)(\mathbf{u}, \mathbf{u}) &= \int_{\Omega} \nu_0 \left( \varepsilon^2 + |\mathbf{D}\mathbf{u}^k|^2 \right)^{\frac{p-2}{2}} (\mathbf{D}\mathbf{u} : \mathbf{D}\mathbf{u}) \, d\mathbf{x} \\
&\quad + \gamma(p-2) \int_{\Omega} \nu_0 \left( \varepsilon^2 + |\mathbf{D}\mathbf{u}^k|^2 \right)^{\frac{p-4}{2}} |\mathbf{D}\mathbf{u}^k : \mathbf{D}\mathbf{u}|^2 \, d\mathbf{x} \\
&\geq \int_{\Omega} \nu_0 \left( \varepsilon^2 + |\mathbf{D}\mathbf{u}^k|^2 \right)^{\frac{p-2}{2}} |\mathbf{D}\mathbf{u}|^2 \, d\mathbf{x} \\
&\quad + \gamma(p-2) \int_{\Omega} \nu_0 \left( \varepsilon^2 + |\mathbf{D}\mathbf{u}^k|^2 \right)^{\frac{p-4}{2}} |\mathbf{D}\mathbf{u}^k|^2 |\mathbf{D}\mathbf{u}|^2 \, d\mathbf{x} \\
&\geq \int_{\Omega} \nu_0 \left( \varepsilon^2 + |\mathbf{D}\mathbf{u}^k|^2 \right)^{\frac{p-2}{2}} |\mathbf{D}\mathbf{u}|^2 \, d\mathbf{x} \\
&\quad + \gamma(p-2) \int_{\Omega} \nu_0 \left( \varepsilon^2 + |\mathbf{D}\mathbf{u}^k|^2 \right)^{\frac{p-2}{2}} |\mathbf{D}\mathbf{u}|^2 \, d\mathbf{x} \\
&= (1 + \gamma(p-2)) \int_{\Omega} \nu_0 \left( \varepsilon^2 + |\mathbf{D}\mathbf{u}^k|^2 \right)^{\frac{p-2}{2}} |\mathbf{D}\mathbf{u}|^2 \, d\mathbf{x}.
\end{aligned}$$

From this, the first inequality follows from using Eq. (5) with the definition of  $\nu_k$  and the second inequality follows from the definition of  $\|\cdot\|_{\infty}$ .

(ii) Again, using that the second term in Eq. (8) is non-positive, we have that

$$\begin{aligned}
a'(\mathbf{u}^k)(\mathbf{u}, \mathbf{u}) &\leq \int_{\Omega} \nu_0 \left( \varepsilon^2 + |\mathbf{D}\mathbf{u}^k|^2 \right)^{\frac{p-2}{2}} |\mathbf{D}\mathbf{u}|^2 \, d\mathbf{x} \\
&\leq \int_{\Omega} \varepsilon^{p-2} |\mathbf{D}\mathbf{u}^k|^2 \, d\mathbf{x} = \nu_{max} \|\mathbf{D}\mathbf{u}\|^2.
\end{aligned}$$

□

**Proposition 1** (Eigenvalue bounds for  $\tilde{S}^{-1}S$ ). *Consider the Stokes problem with power-law fluid Eq. (5) linearized using either the Picard ( $\gamma = 0$ ) or the Newton ( $\gamma = 1$ ) method as in Eq. (9). Let  $\lambda$  denote an eigenvalue of  $\tilde{S}^{-1}S$ , where  $\tilde{S} = M$  or  $\tilde{S} = M_{\nu}$ . The following bounds for  $\lambda$  hold:*

(i) For  $\tilde{S} = M$ :

$$c_0^2 \varepsilon^{2-p} \leq \lambda \leq \frac{(\varepsilon^2 + \|\mathbf{D}\mathbf{u}_h^k\|_{\infty}^2)^{\frac{2-p}{2}}}{\nu_0(1 + \gamma(p-2))}$$

(ii) For  $\tilde{S} = M_\nu$ :

$$c_\nu^2 \leq \lambda \leq \frac{d}{1 + \gamma(p-2)}$$

where  $d = 2, 3$  is the dimension of the problem.

*Proof.* Denoting by  $\langle v, w \rangle = w^\top v$  the Euclidean inner product, we have that

$$\begin{aligned} a'(\mathbf{u}_h^k)(\mathbf{v}_h, \mathbf{v}_h) &= \langle Av, v \rangle, \\ \|q_h\|^2 &= \langle Mq, q \rangle, \\ \|\nu_k^{-1/2} q_h\|^2 &= \langle M_\nu q, q \rangle. \end{aligned}$$

Furthermore, due to the definitions of  $A$  (symmetric positive definite) and  $B$ , we have that

$$\begin{aligned} \langle Sq, q \rangle &= \langle BA^{-1}B^\top q, q \rangle = \langle A^{-1}B^\top q, B^\top q \rangle = \\ &= \sup_{v \in \mathbb{R}^n} \frac{\langle v, B^\top q \rangle^2}{\langle Av, v \rangle} = \sup_{\mathbf{v}_h \in V_h} \frac{(\nabla \cdot \mathbf{v}_h, q_h)^2}{a'(\mathbf{u}_h^k)(\mathbf{v}_h, \mathbf{v}_h)}. \end{aligned} \quad (20)$$

Proof of (i): From Lemma 2(i) followed by Lemma 1(i) and Cauchy-Schwartz inequality we have that:

$$\begin{aligned} \sup_{\mathbf{v}_h \in V_h} \frac{(\nabla \cdot \mathbf{v}_h, q_h)^2}{a'(\mathbf{u}_h^k)(\mathbf{v}_h, \mathbf{v}_h)} &\leq \sup_{\mathbf{v}_h \in V_h} \frac{(\varepsilon^2 + \|\mathbf{D}\mathbf{u}_h^k\|_\infty^2)^{\frac{2-p}{2}} (\nabla \cdot \mathbf{v}_h, q_h)^2}{\nu_0(1 + \gamma(p-2)) \|\mathbf{D}\mathbf{v}_h\|^2} \\ &\leq \sup_{\mathbf{v}_h \in V_h} \frac{(\varepsilon^2 + \|\mathbf{D}\mathbf{u}_h^k\|_\infty^2)^{\frac{2-p}{2}} (\nabla \cdot \mathbf{v}_h, q_h)^2}{\nu_0(1 + \gamma(p-2)) \|\nabla \cdot \mathbf{v}_h\|^2} \\ &\leq \sup_{\mathbf{v}_h \in V_h} \frac{(\varepsilon^2 + \|\mathbf{D}\mathbf{u}_h^k\|_\infty^2)^{\frac{2-p}{2}} \|\nabla \cdot \mathbf{v}_h\|^2 \|q_h\|^2}{\nu_0(1 + \gamma(p-2)) \|\nabla \cdot \mathbf{v}_h\|^2} \\ &\leq \frac{(\varepsilon^2 + \|\mathbf{D}\mathbf{u}_h^k\|_\infty^2)^{\frac{2-p}{2}}}{\nu_0(1 + \gamma(p-2))} \langle Mq_h, q_h \rangle, \end{aligned}$$

which together with Eq. (20) gives the upper bound of (i). Similarly the lower bound can be derived by using Lemma 2(ii), followed by Lemma 1(i) and Eq. (10):

$$\sup_{\mathbf{v}_h \in V_h} \frac{(\nabla \cdot \mathbf{v}_h, q_h)^2}{a'(\mathbf{u}_h^k)(\mathbf{v}_h, \mathbf{v}_h)} \geq \sup_{\mathbf{v}_h \in V_h} \frac{(\nabla \cdot \mathbf{v}_h, q_h)^2}{\nu_{max} \|\mathbf{D}\mathbf{v}_h\|^2} \geq \sup_{\mathbf{v}_h \in V_h} \frac{(\nabla \cdot \mathbf{v}_h, q_h)^2}{\nu_{max} \|\nabla \mathbf{v}_h\|^2} \geq \frac{c_0^2}{\varepsilon^{p-2}} \langle Mq, q \rangle.$$

Proof of (ii): From Lemma 2(i), followed by the Cauchy-Schwartz inequality and Lemma 1(ii) we have that

$$\begin{aligned}
\sup_{\mathbf{v}_h \in V_h} \frac{(\nabla \cdot \mathbf{v}_h, q_h)^2}{a'(\mathbf{u}_h^k)(\mathbf{v}_h, \mathbf{v}_h)} &\leq \sup_{\mathbf{v}_h \in V_h} \frac{(\nu_k^{1/2} \nabla \cdot \mathbf{v}_h, \nu_k^{-1/2} q_h)^2}{(1 + \gamma(p-2)) \|\nu_k^{1/2} \mathbf{D}\mathbf{v}_h\|^2} \\
&\leq \sup_{\mathbf{v}_h \in V_h} \frac{\|\nu_k^{1/2} \nabla \cdot \mathbf{v}_h\|^2 \|\nu_k^{-1/2} q_h\|^2}{(1 + \gamma(p-2)) \|\nu_k^{1/2} \mathbf{D}\mathbf{v}_h\|^2} \\
&\leq \sup_{\mathbf{v}_h \in V_h} \frac{d \|\nu_k^{1/2} \mathbf{D}\mathbf{v}_h\|^2 \|\nu_k^{-1/2} q_h\|^2}{(1 + \gamma(p-2)) \|\nu_k^{1/2} \mathbf{D}\mathbf{v}_h\|^2} \\
&\leq \frac{d}{(1 + \gamma(p-2))} \langle M_\nu q, q \rangle,
\end{aligned}$$

which together with Eq. (20) gives the upper bound of (ii). The lower bound can be derived using Lemma 2(ii) and the auxiliary *inf-sup* condition in Eq. (17)

$$\sup_{\mathbf{v}_h \in V_h} \frac{(\nabla \cdot \mathbf{v}_h, q_h)^2}{a'(\mathbf{u}_h^k)(\mathbf{v}_h, \mathbf{v}_h)} \geq \sup_{\mathbf{v}_h \in V_h} \frac{(\nabla \cdot \mathbf{v}_h, q_h)^2}{\|\nu_k^{1/2} \mathbf{D}\mathbf{v}_h\|^2} \geq c_\nu^2 \langle M_\nu q, q \rangle,$$

which, together with Eq. (20), gives the lower bound of (ii).  $\square$

**Remark 2.** The constants  $c_0$  and  $c_\nu$  will be determined numerically, see Section 4.1. The constant  $c_0$  is independent of  $\varepsilon$ , while theoretical results from Grinevich and Olshanskii [2009] imply that  $c_\nu$  will only weakly depend on  $\varepsilon$ .

**Remark 3.** For the classical preconditioner  $\tilde{S} = M$  the lower bound is proportional to power of  $\varepsilon$  (given that  $p < 2$ ) and the upper bound depends on  $\varepsilon$  and the maximum value of the strain rate in such a way that the bound for the ratio  $\lambda_{\max}/\lambda_{\min}$  increases for as  $\varepsilon$  becomes smaller. This is, in general, bad for the performance of linear solvers. The choice  $\tilde{S} = M_\nu$  is clearly better as it has a constant upper bound and the lower bound has, as shown in Grinevich and Olshanskii [2009], a much weaker dependence on  $\varepsilon$ . The Picard method ( $\gamma = 0$ ) results in a slightly lower bound for  $\lambda_{\max}$ , however, the better non-linear convergence properties of the Newton method will for most applications likely make the Newton method the overall faster option.

#### 4.1 Determining the *inf-sup* constants $c_0$ and $c_\nu$

To investigate how the eigenvalue bounds from Section 4 relate to numerically computed eigenvalues (Section 5), we compute the two *inf-sup* constants  $c_0$  and  $c_\nu$  numerically.

We follow the method presented in Qin [1994], Arnold and Rognes [2009] and make use of and modify the software ASCoT [Rognes, 2009] which is Python module built on top of the FEniCS framework [Alnæs et al., 2015] that automates the testing of stability conditions like those in Eqs. (10) and (17). The *inf-sup* is the square root of the minimum eigenvalue for the following generalized eigenvalue problem: find  $0 \neq (\mathbf{u}_h, \pi_h) \in V_h \times Q_h$  so that

$$\langle \mathbf{u}_h, \mathbf{v}_h \rangle_V + b(\mathbf{v}_h, \pi_h) + b(\mathbf{u}_h, q) = -\lambda \langle \pi_h, q \rangle_Q, \quad \forall (\mathbf{v}_h, q) \in V_h \times Q_h$$

where  $\langle \cdot, \cdot \rangle_{V,Q}$  represents the inner product on the velocity and pressure space, respectively, that induces the norms used in the two separate *inf-sup* conditions Eqs. (10) and (17). For the numerical computation of  $c_\nu$ , we make the assumption that the above variational formulation, proven in Qin [e.g., 1994] for  $c_0$ , also holds for  $c_\nu$ . The discrete eigenvalue problem is solved using SLEPc [Hernandez et al., 2005, Roman et al., 2022] with appropriate restrictions, such as basis for the nullspace consisting of the constant functions in the case of pure Dirichlet conditions.

### 5 Numerical Experiments

In this section we numerically confirm that the bounds of Proposition 1 hold. Since the bounds depend on  $\varepsilon$ , a parameter that should be as small as possible in ice-sheet models, we study how the eigenvalues vary with  $\varepsilon$ . We run experiments using Picard and Newton iterations for both  $P2P1$  elements and MINI-elements. All simulations are performed using an in-house Python module built on top of the FEniCS framework [Alnæs et al., 2015, Logg et al., 2012] compiled with SLEPc [Hernandez et al., 2005, Roman et al., 2022] as a backend.

To compute the eigenvalues of  $\tilde{S}^{-1}S$  we assemble the matrices  $\tilde{S}, B, B^\top$  and  $A$  and explicitly compute the inverses  $A^{-1}$  to assemble  $S = BA^{-1}B^\top$ . The generalized eigenvalue problem

$$Sx = \lambda \tilde{S}x \tag{21}$$

is then solved using SLEPc. Given the expensive operation of directly computing  $A^{-1}$ , we only assemble the matrices and solve for the eigenvalues

in the last Picard or Newton iteration, i.e., in the iteration for which the method has converged to a given tolerance. The method is considered to have convergence when a tolerance of relative tolerance  $r_{tol} = 10^{-6}$  or absolute tolerance  $a_{tol} = 10^{-10}$  has been reached. At the time of convergence, the solution  $(\mathbf{u}, \pi)$  together the in the non-linear iteration computed represent the final state of the system, so we deem this approach to be sufficient for investigating the theoretical bounds. We, however, in a few cases computed the eigenvalues for Eq. (21) for every iteration in a simulation run: the outcomes of these did not change any of the results compared to the last iteration.

The system in each non-linear iteration is solved with PETSc Balay et al. [1997, 2016] using GMRES [Saad and Schultz, 1986] preconditioned by  $P$  with either  $\tilde{S} = M$  or  $\tilde{S} = M_\nu$  (Eq. (14)), with the action of  $P^{-1}$  approximated using AMG [Henson and Yang, 2002].

## 5.1 Model problems

### 5.1.1 A manufactured solution for power-law fluids

We use the manufactured solution (MS) presented in Belenki et al. [2012] to solve the Dirichlet problem Eq. (3a) in two dimensions on the domain  $(x, y) \in [-1, 1] \times [-1, 1]$ . The right-hand side and Dirichlet boundary conditions are given by inserting the specified solution of the problem,

$$\mathbf{u} = |(x, y)|^{a-1}(x, -y)^\top, \quad \pi = |(x, y)|^b, \quad (22)$$

into Eq. (3a). For the solution Eq. (22) to be regular enough it is required that  $a > 1$  and  $b > -1 + \frac{2}{p}$ . The manufactured solution allows us to make sure that 1) our solution is correct, and 2) control the regularity of the problem. Since we want to ensure that our results hold for challenging problems we follow [Belenki et al., 2012] and set  $a = 1 + \delta$  and  $b = -1 + \frac{2}{p} + \delta$  with  $\delta = 0.01$ , specifying the solution to be of very low regularity. The material parameters are set to  $\nu_0 = 1$  and  $p = 4/3$ .

The square domain is discretized using a structured mesh which subdivides each side in  $nx$  sections, where the resulting rectangles are diagonally cut to form  $2(nx)^2$  triangle elements. The typical mesh in this experiment used  $nx = 32$ , resulting in 2048 elements. The initial guess starting the non-linear iteration is zero when using the Picard method, while the Newton method uses an initial guess solved for using the Picard method with a low relative tolerance ( $r_{tol} = 10^{-2}$ ) for 5 iterations.

### 5.1.2 A glacial-ice benchmark experiment

To investigate how well the theory applies to practical ice-modeling examples we run the classical benchmark experiment ISMIP-HOM E, which consists of a stationary simulation of Haut Glacier d’Arolla situated in the Swiss alps [Pattyn et al., 2008], see Fig. 1. The glacier boundary  $\Gamma$  consists of the

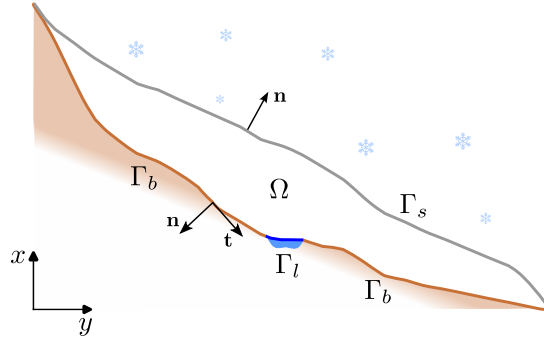


Figure 1: A conceptual cross section of Haut Glacier d’Arolla, the domain used for experiment Arolla. The boundary of the domain  $\Gamma$  is subdivided into the glacier surface  $\Gamma_s$  (gray line) and the base of the ice which rests partly on bedrock ( $\Gamma_b$ , brown line) and partly on a subglacial lake ( $\Gamma_l$ , blue line).

ice/atmosphere interface  $\Gamma_s$  and ice/bedrock interface  $\Gamma_b$ . The ice velocity and pressure is given as the solution to Eq. (3a) with  $p = 4/3$ ,  $\nu_0$  set to a typical value used for simulations of isothermal ice,  $\mathbf{f} = \rho \mathbf{\hat{g}}$  and with appropriately modified boundary conditions. Over the subglacial lake,  $\Gamma_l$ , a Navier-slip condition applies with an impenetrability condition in the normal direction and free slip in the tangential direction, while a no-slip condition applies to the rest of the bed  $\Gamma_b$ . At the ice surface,  $\Gamma_s$ , a stress-free condition applies. If we by  $\mathbf{n}$  and  $\mathbf{t}$  denote the to the boundary outward-pointing unit normal and tangential vectors, respectively, the boundary conditions can be summarized as:

$$\mathbf{u} \cdot \mathbf{n} = 0 \text{ on } \Gamma_l, \quad (23a)$$

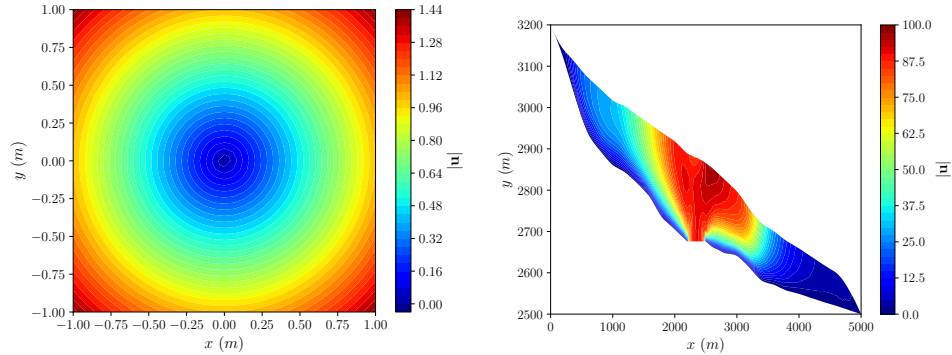
$$\mathbf{t} \cdot \mathbf{S} \cdot \mathbf{n} = 0 \text{ on } \Gamma_l, \quad (23b)$$

$$(\mathbf{S} - \pi \mathbf{I}) \cdot \mathbf{n} = \mathbf{0} \text{ on } \Gamma_s, \quad (23c)$$

$$\mathbf{u} = \mathbf{0} \text{ on } \Gamma_b, . \quad (23d)$$

The impenetrability condition Eq. (23a) is here implemented strongly through a local rotation of the coordinate system in the direction of a discrete normal average of neighboring cell facets at the degree of freedom [John, 2002, Råback et al., 2022]. The boundary conditions Eqs. (23b) and (23c) are both natural boundary conditions that are weakly implemented through the variational formulation, while Eq. (23d) is a Dirichlet condition on the velocity.

The unstructured mesh used to discretize the Haut Glacier d’Arolla experiment is the result of a Delauney triangulation of the domain using **Gmsh** [Geuzaine and Remacle, 2009], with the characteristic mesh size,  $lc$ , being a measure of the typical cell size (longest edge of a triangle) of the mesh. The typical mesh used in this experiment consists of 1620 triangles with  $lc = 32$ . The initial guess starting the non-linear iteration is zero using both the Picard and Newton method.



(a) Simulated speed,  $|\mathbf{u}|$ , for the MS with low regularity experiment using  $P2P1$  (b) Simulated speed,  $|\mathbf{u}|$ , for the Arolla experiment using  $P2P1$

Figure 2: Simulation results from the two experiments: manufactured solution (MS) with low regularity and Haut Glacier d’Arolla (Arolla). The colors shows the magnitude of the velocity,  $|\mathbf{u}|$ .

## 5.2 Results for $\tilde{S} = M$

The theoretical upper and lower eigenvalue bounds, using the numerically computed  $c_0$ , for  $M^{-1}S$  in the final Newton iteration are shown in red dashed and green dotted lines, respectively, in Fig. 3, and computed largest and smallest eigenvalues are shown as up and down triangle markers, respectively ( $\lambda_{max}$  in red and  $\lambda_{min}$  in green). Theory predicts that the lowest eigenvalue  $\lambda_{min}$  decreases with  $\varepsilon$  while the largest eigenvalue should be bounded from



below. This leads to a large ratio  $\lambda_{max}/\lambda_{min}$  ( $10^4$ - $10^6$  for the glacier) which in general leads to bad performance of linear solvers. For the manufactured problem Eq. (22) theory and experiments align very well for  $\lambda_{max}$ , while the experimentally computed  $\lambda_{min}$  are larger than the theoretical bound predicts for the manufactured problem. We believe this is due to that there is an unresolved very localized peak in the viscosity for the manufactured problem. On Haut Glacier d’Arolla the viscosity is high in a more distributed area around the ice/atmosphere interface, and so theory and experiments align very well for  $P2P1$  elements. The MINI elements result in a significantly lower value for  $c_0$  for the Arolla domain and resulting lower theoretical bounds for  $\lambda_{min}$ . The small value for  $c_0$  is related to the locally poor quality of elements close in parts of the domain at this mesh resolution (see Section 5.4) and most likely leads to small enough eigenvalues that numerical errors of the eigenvalue computations become significant (Fig. 3d).

In addition to the Arolla experiment, we performed simulations with only no-slip (Dirichlet) boundary conditions at the bed, i.e., we set  $\Gamma_l = \emptyset$ : we found no significant change comparing the results of these simulations to Arolla indicating that the boundary conditions, at least in this case, do not have a significant impact on the character of the preconditioned system, but that the results are rather affected by the value of  $c_0$  and the strong dependence on  $\varepsilon$ .

### 5.3 Results for $\tilde{S} = M_\nu$

As expected from theory, the eigenvalues are independent of  $\varepsilon$  for the choice  $\tilde{S} = M_\nu$ , see Fig. 4. Theory and experiments agree very well. Using  $P2P1$  elements the ratio  $\lambda_{max}/\lambda_{min}$  is smaller than  $10^1$  for both the manufactured problem and Haut Glacier d’Arolla, which is beneficial for linear solvers. Using MINI elements for the glacier simulation does however result in a fairly large ratio  $\lambda_{max}/\lambda_{min}$ . This has to do with the value of  $c_0$ , which is affected by e.g., mesh quality, and will be explored more in the next section.

### 5.4 Mesh quality and MINI elements

To further investigate how the smallest eigenvalues using MINI elements are affected by mesh quality, we below present results that show how the *inf-sup* constant  $c_\nu$  is affected by the mesh quality.

Fig. 5 shows the eigenvalue bounds for both experiments using the  $P2P1$  element indicating that these are independent of the mesh sizes  $nx$  and  $lc$ . For the MS experiment using MINI elements give very similar results.

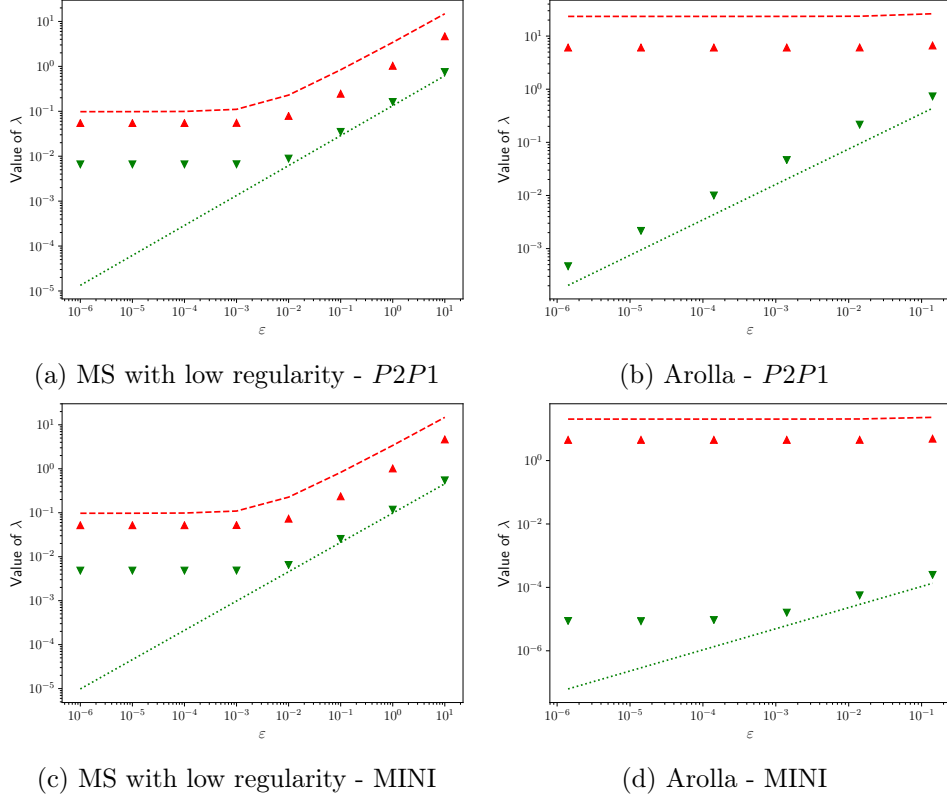


Figure 3: Eigenvalues of  $M^{-1}S$  and their dependency on the regularization parameter  $\varepsilon$  for the experiments using the manufactured solution (MS) with low regularity and Haut Glacier d’Arolla (Arolla). The simulations are performed using the Newton method ( $\gamma = 1$ ) and computations are made at the final non-linear iteration. The theoretical lower and upper eigenvalue bounds,  $c_0^2 \varepsilon^{2-p} \leq \lambda \leq \frac{3}{\nu_0} (\varepsilon^2 + \|\mathbf{Du}_h^k\|_\infty^2)^{\frac{p-2}{2}}$ , are shown as dotted green and dashed red lines, respectively (Proposition 1(i) with  $\gamma = 1$  and  $p = 4/3$ ). Computed smallest non-zero,  $\lambda_{min}$ , and largest,  $\lambda_{max}$ , eigenvalues are shown as green down and red up triangles, respectively.

However, for the unstructured mesh used in Arolla, the minimum eigenvalue  $\lambda_{min}$  can be seen to decrease with a finer mesh sizes, see Fig. 6a.

A reasonable explanation for this behavior is the locally reduced mesh quality that occurs when using an finer unstructured triangulation around the cusp-like geometry at the head of glacier (see Fig. 1). Compared to  $P2P1$ , using MINI with low-quality elements has a more significant impact

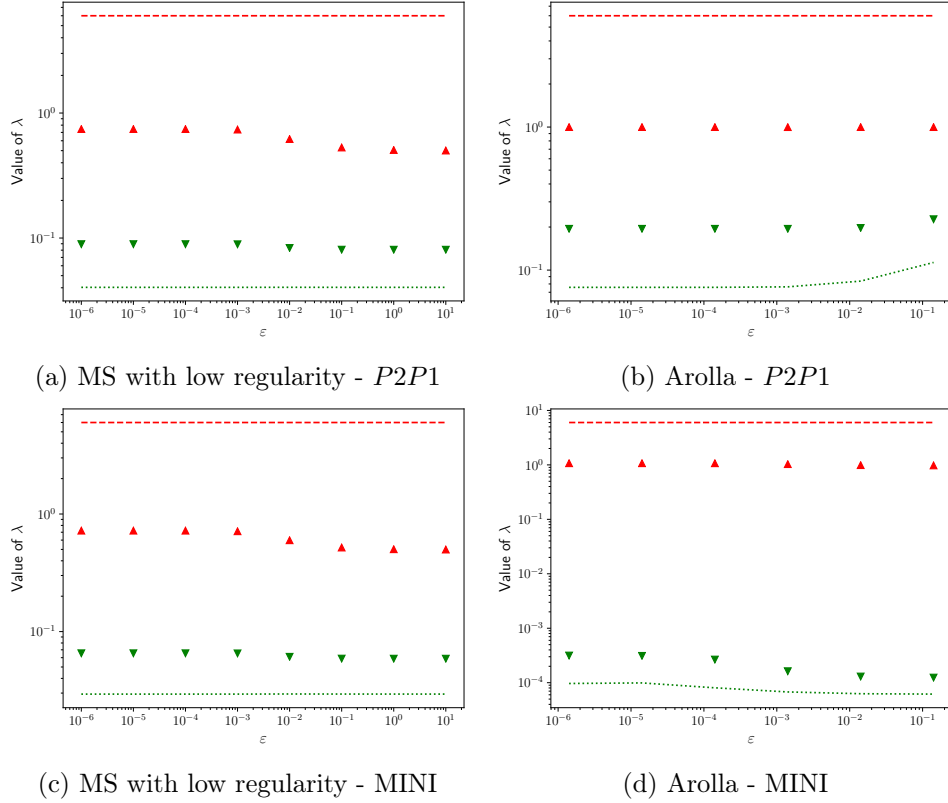


Figure 4: Eigenvalues of  $M_\nu^{-1}S$  and their dependency on the regularization parameter  $\varepsilon$  for the experiments using the manufactured solution (MS) with low regularity and Haut Glacier d’Arolla (Arolla). Colors and markers as in Fig. 3, except for the theoretical eigenvalue bounds which for  $M_\nu^{-1}S$  are  $c_\nu^2 \leq \lambda \leq 6$  (Proposition 1(ii) with  $\gamma = 1$  and  $p = 4/3$ ).

on the *inf-sup* constant  $c_0$ , which auxiliary *inf-sup* constant  $c_\nu$  depends on. The degradation of  $\lambda_{min}$  shown in Fig. 6a is most likely the result of the lower stability properties inherent in the MINI element. To support this view, we perform a simulation using a vertically extruded mesh (extrusion in 7 layers from bed to surface): such a mesh does not resolve the cusp-like feature as well, but results in elements of better quality (larger ratio of minimum/maximum element angles). Such extruded meshes are very common in large-scale ice-sheet models and are therefore of interest. Fig. 6b shows the independence of the eigenvalues of the regularization parameter  $\varepsilon$  for a simulation using an extruded mesh consisting of 1792 elements, approximately

equal the amount of elements as the unstructured mesh with  $lc = 32$ .

The numerical results presented above suggest that the *inf-sup* constant  $c_\nu$  in practice is very weakly dependent on, if not nearly independent of, the regularization parameter  $\varepsilon$ , but is directly connected through the dependence of  $c_\nu$  to the regular *inf-sup* constant  $c_0$  (see Table 1). If so, the quality of  $M_\nu$  as a preconditioner would be related to the stability qualities of a specific *inf-sup* stable element, e.g., *P2P1* or MINI.

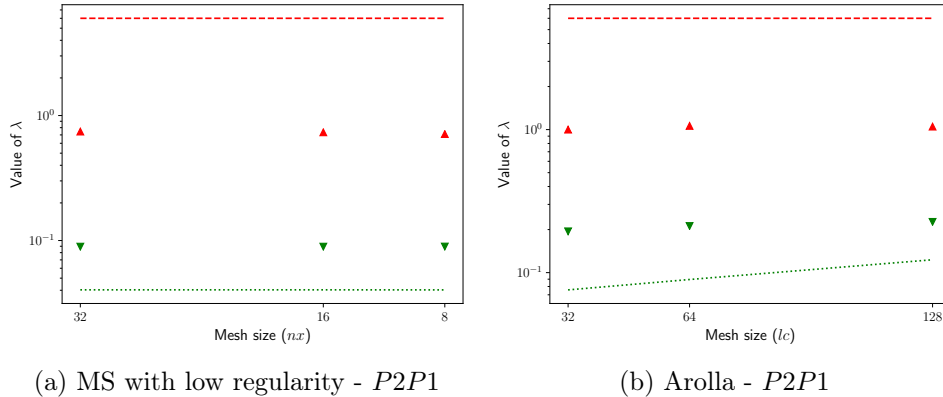


Figure 5: Eigenvalues of  $M_\nu^{-1}S$  and their dependency on mesh size  $nx$  and  $lc$  for the experiments using the manufactured solution (MS) with low regularity and Haut Glacier d’Arolla (Arolla), respectively. Mesh size is finer to the left. Colors and markers as in Fig. 4.

## 6 Summary and Conclusion

In this study we consider Schur-block preconditioners for the discretized  $p$ -Stokes equations for fluids with shear-dependent viscosity. In particular, we focus on the regularized constitutive equation for the power-law fluid ice, which has no explicit lower bound for the viscosity and an upper bound inversely proportional to the regularization parameter  $\varepsilon$ . Based on previous results in Grinevich and Olshanskii [2009], He et al. [2015] we adapt the theory to the considered power-law fluid and derive bounds of the eigenvalues of the preconditioned Schur block using either the mass matrix,  $M$ , or the viscosity-scaled mass matrix,  $M_\nu$ . Both the Newton and the Picard method are considered. For  $M$  the lower bound for the eigenvalues depends directly on  $\varepsilon$  and the upper bound on the maximum strain rate solved for in the previous non-linear iteration. For  $M_\nu$  the lower bound depends only weakly and

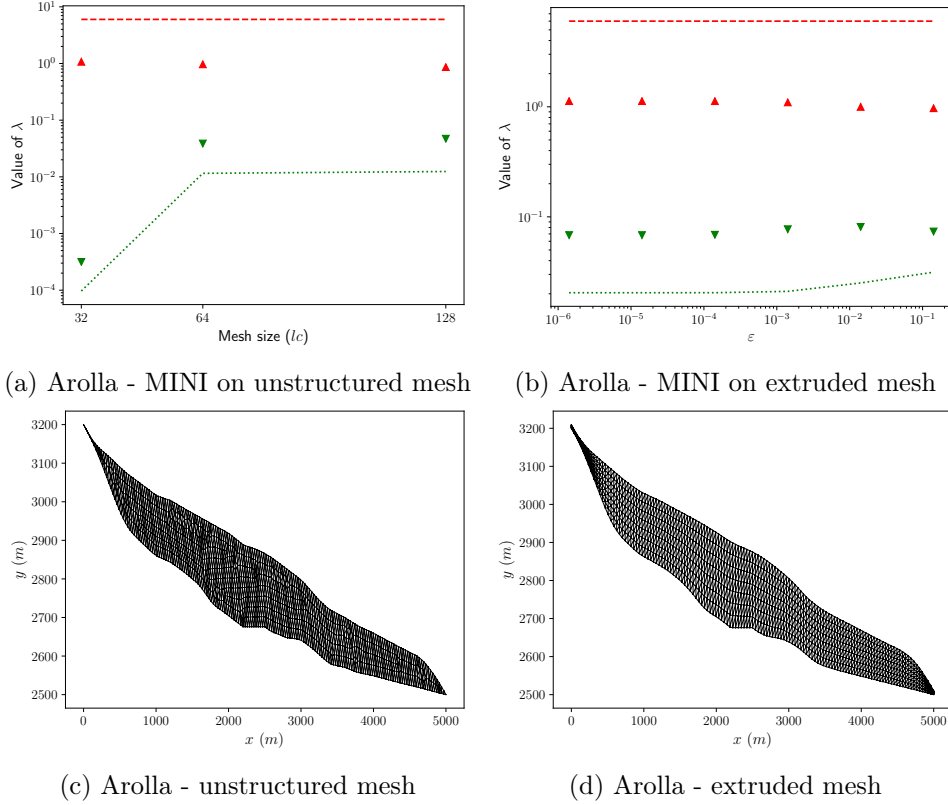


Figure 6: Eigenvalues of  $M_\nu^{-1}S$  for the Haut Glacier d'Arolla (Arolla) experiment. Top panel (colors and markers as in Fig. 4): (a) shows the dependency of the eigenvalues on the mesh size  $lc$  when using an unstructured mesh. The finest mesh size is  $lc = 32$ . (b) shows the dependency of the eigenvalues on the regularization parameter  $\varepsilon$  using an extruded mesh with similar mesh size to  $lc = 32$  (total number of elements in the triangulations are approximately equal). The bottom panel shows the unstructured (c) and extruded (d) meshes, respectively.

indirectly, as shown Grinevich and Olshanskii [2009], on  $\varepsilon$  while the upper bound is constant dependent of the given problem dimension for the Picard method and for Newton method additionally dependent on the value of  $p$ . Hence, using  $M_\nu$  results in a better clustering of eigenvalues for both the Picard and Newton method. Eigenvalues computed in numerical experiments show close agreement with the theoretical bounds presented. Furthermore, numerically computed eigenvalue bounds suggest that the lower eigenvalue

bound for the  $M_\nu$ -preconditioned system is nearly independent of  $\varepsilon$ , further confirming the theoretical results from Grinevich and Olshanskii [2009]. The numerical experiments indicate that the lower bounds for  $M_\nu$  depend more directly on the classical LBB *inf-sup* connected to the domain and stability properties of a specific finite element. For MINI elements this suggests that the efficiency of the preconditioner depends on the quality of the mesh, which is particularly relevant to large-scale ice-sheet simulations, in which MINI elements are commonly used.

### Acknowledgments

The authors would like to thank Prof. M. Olshanskii for kindly answering our questions regarding the original theory presented in Grinevich and Olshanskii [2009]. Funding for this research was provided by the Swedish e-Science Research Centre (SeRC). The authors declare that they have no known competing financial interests or personal relationships that could have appeared to influence the work reported in this paper.

### References

- M. Alnæs, J. Blechta, J. Hake, A. Johansson, B. Kehlet, A. Logg, C. Richardson, J. Ring, M. Rognes, and G. Wells. The FEniCS project version 1.5. *Archive of Numerical Software*, 3(100), 2015. ISSN 2197-8263. doi: 10.11588/ans.2015.100.20553. URL <http://journals.ub.uni-heidelberg.de/index.php/ans/article/view/20553>.
- D. Arnold and M. Rognes. Stability of lagrange elements for the mixed laplacian. *Calcolo*, 46:245–260, 07 2009. doi: 10.1007/s10092-009-0009-6.
- I. Babuška. The finite element method with Lagrangian multipliers. *Numer. Math.*, 20(3):179–192, 1973.
- C. Baiocchi, F. Brezzi, and L. P. Franca. Virtual bubbles and Galerkin-least-squares type methods (Ga.L.S.). *Comput. Methods in Appl. Mech. Eng.*, 105(1):125 – 141, 1993. doi: [https://doi.org/10.1016/0045-7825\(93\)90119-I](https://doi.org/10.1016/0045-7825(93)90119-I).
- S. Balay, W. D. Gropp, L. C. McInnes, and B. F. Smith. Efficient management of parallelism in object oriented numerical software libraries. In E. Arge, A. M. Bruaset, and H. P. Langtangen, editors, *Modern Software Tools in Scientific Computing*, pages 163–202. Birkhäuser Press, 1997.

- S. Balay, S. Abhyankar, M. F. Adams, J. Brown, P. Brune, K. Buschelman, L. Dalcin, V. Eijkhout, W. D. Gropp, D. Kaushik, M. G. Knepley, L. C. McInnes, K. Rupp, B. F. Smith, S. Zampini, H. Zhang, and H. Zhang. PETSc Web page. <http://www.mcs.anl.gov/petsc>, 2016. URL <http://www.mcs.anl.gov/petsc>.
- L. Belenki, L. C. Berselli, L. Diening, and M. Růžička. On the finite element approximation of p-Stokes systems. *SIAM J. Numer. Anal.*, 50(2):373–397, 2012. doi: 10.1137/10080436X.
- F. Brezzi. On the Existence, Uniqueness and Approximation of Saddle-Point Problems Arising from Lagrangian Multipliers. *ESAIM-Math. Model. Num.*, 8(R2):129–151, 1974.
- K. M. Cuffey and W. S. B. Paterson. *The physics of glaciers*. Academic Press, 2010.
- P. Duval. The role of the water content on the creep rate of polycrystalline ice. *IAHS Publ.*, 118:29–33, 1977.
- P. Duval, M. F. Ashby, and I. Anderman. Rate-controlling processes in the creep of polycrystalline ice. *J. Phys. Chem.*, 87(21):4066–4074, 1983. doi: 10.1021/j100244a014. URL <http://dx.doi.org/10.1021/j100244a014>.
- H. C. Elman, D. J. Silvester, and A. J. Wathen. *Finite Elements and Fast Iterative Solvers with Applications in Incompressible Fluid Dynamics*. Numerical Mathematics and Scientific Computation. Oxford University Press, 2005. ISBN 0198528671.
- M. R. T. Fraters, W. Bangerth, C. Thieulot, A. C. Glerum, and W. Spakman. Efficient and practical Newton solvers for non-linear Stokes systems in geodynamic problems. *Geophys. J. Int.*, 218(2):873–894, 04 2019. ISSN 0956-540X. doi: 10.1093/gji/ggz183. URL <https://doi.org/10.1093/gji/ggz183>.
- O. Gagliardini, T. Zwinger, F. Gillet-Chaulet, G. Durand, L. Favier, B. de Fleurian, R. Greve, M. Malinen, C. Martín, P. Råback, J. Ruokolainen, M. Sacchetti, M. Schäfer, H. Seddik, and J. Thies. Capabilities and performance of Elmer/Ice, a new generation ice-sheet model. *Geosci. Model Dev.*, 6:1299–1318, 2013a.
- O. Gagliardini, T. Zwinger, F. Gillet-Chaulet, and et al. Capabilities and performance of Elmer/Ice, a new generation ice-sheet model. *Geosci. Model Dev.*, 6:1299–1318, 2013b.

- C. Geuzaine and J.-F. Remacle. Gmsh: A 3-D finite element mesh generator with built-in pre- and post-processing facilities. *Int. J. Numer. Meth. Eng.*, 79(11):1309–1331, 2009.
- J. Glen. The creep of polycrystalline ice. *Proc. Roy. Soc. Lond. A*, 228(1175): 519–538, 1955.
- P. P. Grinevich and M. A. Olshanskii. An iterative method for the Stokes-type problem with variable viscosity. *SIAM J. Sci. Comput.*, 31(5):3959–3978, 2009. doi: 10.1137/08744803. URL <https://doi.org/10.1137/08744803>.
- X. He, M. Neytcheva, and C. Vuik. On preconditioning of incompressible non-Newtonian flow problems. *J. Comput. Math.*, 33(1):33–58, 2015. ISSN 1991-7139. doi: <https://doi.org/10.4208/jcm.1407-m4486>. URL [http://global-sci.org/intro/article\\_detail/jcm/9826.html](http://global-sci.org/intro/article_detail/jcm/9826.html).
- V. E. Henson and U. M. Yang. BoomerAMG: a parallel algebraic multigrid solver and preconditioner. *Appl. Numer. Math.*, 41:155–177, 2002.
- V. Hernandez, J. E. Roman, and V. Vidal. SLEPc: A scalable and flexible toolkit for the solution of eigenvalue problems. *ACM Trans. Math. Software*, 31(3):351–362, 2005.
- A. Hirn. Finite element approximation of singular power-law systems. *Math. Comp.*, 82(283):1247–1268, 2013. ISSN 00255718, 10886842. URL <http://www.jstor.org/stable/42002697>.
- T. Isaac, G. Stadler, and O. Ghattas. Solution of nonlinear stokes equations discretized by high-order finite elements on Nonconforming and anisotropic meshes, with application to ice sheet dynamics. *SIAM J. Sci. Comput.*, 37(6):B804–B833, 2015. doi: 10.1137/140974407. URL <https://doi.org/10.1137/140974407>.
- V. John. Slip with friction and penetration with resistance boundary conditions for the Navier–Stokes equations — numerical tests and aspects of the implementation. *J. Comput. Appl. Math.*, 147(2):287 – 300, 2002. ISSN 0377-0427. doi: [http://dx.doi.org/10.1016/S0377-0427\(02\)00437-5](http://dx.doi.org/10.1016/S0377-0427(02)00437-5). URL <http://www.sciencedirect.com/science/article/pii/S0377042702004375>.
- V. John. *Finite element methods for incompressible flow problems*, volume 51 of *Springer Series in Computational Mathematics*. Springer, 2016. ISBN



3319457497 9783319457499. doi: 10.1007/978-3-319-45750-5. URL <https://link.springer.com/book/10.1007%2F978-3-319-45750-5>.

K. Kaiser. Finite element methods for the incompressible Stokes equations with non-constant viscosity. Master’s thesis, Berlin Mathematical School, Freie Universität, Berlin, Germany, 01 2014.

W. Leng, L. Ju, M. Gunzburger, S. Price, and T. Ringler. A parallel high-order accurate finite element nonlinear Stokes ice sheet model and benchmark experiments. *J. Geophys. Res.: Earth Surface*, 117(F1), 2012. ISSN 2156-2202. doi: 10.1029/2011JF001962. URL <http://dx.doi.org/10.1029/2011JF001962>. F01001.

A. Logg, K.-A. Mardal, and G. N. Wells. *Automated Solution of Differential Equations by the Finite Element Method*, volume 84 of *Lecture Notes in Computational Science and Engineering*. Springer, 2012. doi: 10.1007/978-3-642-23099-8. URL <http://dx.doi.org/10.1007/978-3-642-23099-8>.

M. Malinen, J. Ruokolainen, P. Råback, J. Thies, and T. Zwinger. Parallel block preconditioning by using the solver of Elmer. pages 545–547, 06 2012. ISBN 978-3-642-36802-8. doi: 10.1007/978-3-642-36803-5\_43.

D. May, J. Brown, and L. Le Pourhiet. A scalable, matrix-free multigrid preconditioner for finite element discretizations of heterogeneous stokes flow. *Comput. Methods Appl. Mech. Eng.*, 290:496–523, 2015. ISSN 0045-7825. doi: <https://doi.org/10.1016/j.cma.2015.03.014>. URL <https://www.sciencedirect.com/science/article/pii/S0045782515001243>.

F. Pattyn, L. Perichon, A. Aschwanden, B. Breuer, B. de Smedt, O. Gagliardini, G. H. Gudmundsson, R. Hindmarsh, A. Hubbard, J. V. Johnson, T. Kleiner, Y. Konovalov, C. Martin, A. J. Payne, D. Pollard, S. Price, M. Rückamp, F. Saito, O. Souček, S. Sugiyama, and T. Zwinger. Benchmark experiments for higher-order and full-Stokes ice sheet models (ISMIP-HOM). *Cryosphere*, 2:95–108, 2008.

H.-O. Pörtner, D. Roberts, and et al. (eds.). *IPCC Special Report on the Ocean and Cryosphere in a Changing Climate*. Cambridge University Press, 2019.

J. Qin. *On the convergence of some low order mixed finite elements for incompressible fluids*. PhD thesis, Dept. of Mathematics, The Pennsylvania State University, 01 1994.

- P. Råback, M. Malinen, J. Ruokalainen, A. Pursula, and T. Zwinger. *Elmer Models Manual*. CSC – IT Center for Science, Helsinki, Finland, 2022.
- M. E. Rognes. Automated stability condition tester (ASCoT), 2009. URL <https://launchpad.net/ascot>.
- J. E. Roman, C. Campos, L. Dalcin, E. Romero, and A. Tomas. SLEPc users manual. Technical Report DSIC-II/24/02 - Revision 3.18, D. Sistemes Informàtics i Computació, Universitat Politècnica de València, 2022.
- M. Rückamp, T. Kleiner, and A. Humbert. Comparison of ice dynamics using full-stokes and blatter–pattyn approximation: application to the north-east greenland ice stream. *The Cryosphere*, 16(5):1675–1696, 2022. doi: 10.5194/tc-16-1675-2022. URL <https://tc.copernicus.org/articles/16/1675/2022/>.
- J. Rudi, G. Stadler, and O. Ghattas. Weighted BFBT preconditioner for Stokes flow problems with highly heterogeneous viscosity. *SIAM J. Sci. Comput.*, 39(5):S272–S297, 2017. doi: 10.1137/16M108450X. URL <https://doi.org/10.1137/16M108450X>.
- Y. Saad and M. H. Schultz. GMRES: A generalized minimal residual algorithm for solving nonsymmetric linear systems. *SIAM J. Sci. Stat. Comput.*, 7(3):856–869, jul 1986. ISSN 0196-5204.
- C. Schannwell, R. Drews, T. A. Ehlers, O. Eisen, C. Mayer, M. Malinen, E. C. Smith, and H. Eisermann. Quantifying the effect of ocean bed properties on ice sheet geometry over 40 000 years with a full-Stokes model. *The Cryosphere*, 14(11):3917–3934, 2020. doi: 10.5194/tc-14-3917-2020. URL <https://tc.copernicus.org/articles/14/3917/2020/>.
- H. Seddik, R. Greve, T. Zwinger, F. Gillet-Chaulet, and O. Gagliardini. Simulations of the Greenland ice sheet 100 years into the future with the full Stokes model Elmer/Ice. *J. Glaciol.*, 58(209):427–440, 2012. doi: 10.3189/2012JoG11J177.
- H. Seroussi, S. Nowicki, and et al. ISMIP6 Antarctica: a multi-model ensemble of the Antarctic ice sheet evolution over the 21st century. *The Cryosphere*, 14(9):3033–3070, 2020. doi: 10.5194/tc-14-3033-2020. URL <https://tc.copernicus.org/articles/14/3033/2020/>.
- Y.-h. Shih, G. Stadler, and F. Wechsung. Robust multigrid techniques for augmented Lagrangian preconditioning of incompressible Stokes equations

with extreme viscosity variations, 2021. URL <https://arxiv.org/abs/2107.00820>.

C. Taylor and P. Hood. Navier-Stokes equations using mixed interpolation. *Int. Symp. on Finite Element Methods in Flow Problems*, pages 121–132, 1974.

H. Zhang, L. Ju, M. Gunzburger, T. Ringler, and S. Price. Coupled models and parallel simulations for three-dimensional full-Stokes ice sheet modeling. *Numer. Math. Theor. Meth. Appl.*, 4:359–381, 2011.

## Appendix A

Table 1 show how the value of the *inf-sup* constants  $c_\nu$  and  $c_0$  vary with mesh size ( $lc$ ) for the Arolla experiment using MINI elements. The strong correlations between  $c_\nu$  and  $c_0$  indicates that the dependence of  $c_\nu$  on the regularization parameter  $\varepsilon$  is as suggested in Grinevich and Olshanskii [2009] very weak.

Table 1: Dependence of the *inf-sup* constants  $c_\nu$  and  $c_0$  on mesh size for the Arolla on unstructured mesh using MINI elements.

$lc$	32	64	128
$c_0$	0.012	0.085	0.146
$c_\nu$	0.010	0.107	0.111